DOI: 10.1002/ente.201200009

Examining the Cu–Mn–O Spinel System as an Oxygen Carrier in Chemical Looping Combustion

Abdul-Majeed Azad,*[a] Ali Hedayati,[b] Magnus Rydén,[c] Henrik Leion,[b] and Tobias Mattisson[c]

Chemical-looping combustion (CLC) and chemical-looping combustion with oxygen uncoupling (CLOU) are attractive alternatives to conventional combustion that provide efficient and direct separation of CO_2. Both processes use metal oxides as oxygen carriers to transfer oxygen between two reactor vessels: the air and fuel reactors. Although monometallic oxides (such as Mn_3O_4, Fe_2O_3, NiO, and CuO) have been successfully employed as oxygen carriers, double oxides of the general formula $Cu_xMn_{3-x}O_4$ in the CuO–Mn_2O_3 system are examined in this work. The carrier was produced by mixing, extruding, and calcining a 1:1 molar (30.8:69.2 mass ratio) mixture of CuO and Mn_2O_3 at 950 °C for 6 or 12 h in static air. XRD analysis revealed that spinels of the general formula $Cu_xMn_{3-x}O_4$ were formed with $0.1 \le x \le 2.5$ in which $x = 3\,Cu/(Cu+Mn)$. The chemical-looping performance was evaluated in a laboratory-scale fluidized-bed reactor from 800–850 °C over several alternating redox cycles using CH_4 as the fuel. The oxygen carrier exhibited reproducible and stable reactivity behavior for both reducing and oxidizing periods in this temperature range. This characteristic makes the system an ideal oxygen-carrier material for CLOU. Moreover, the spinels in the $Cu_xMn_{3-x}O_4$ series are endowed with favorable physicochemical attributes (such as fast redox processes, high crushing strength, and demonstrated CLOU behavior) and may be viable alternatives to CuO–Cu_2O and Mn_2O_3–Mn_3O_4 as potential CLOU materials.

Introduction

According to the intergovernmental panel on climate control (IPCC), a 50–85% reduction in total CO_2 emission by 2050 is mandated to limit the anticipated rise in global temperature to within 2 °C.[1] A number of alternative technologies have been proposed to mitigate the rising levels of CO_2 in the atmosphere. Among these, carbon capture and storage (CCS) is one of the most attractive and viable.

Chemical-looping combustion (CLC) is a promising pathway for efficient CO_2 capture at low cost from gaseous fuels, such as natural gas, syngas, and gasified biomass. The general principles were laid out in the 1950s,[2] but most of the work that concerned the technology was conducted in the last decade.[3–6]

In CLC, fuel is oxidized with oxygen provided by solid oxygen-carrier particles rather than with O_2 direct from air. In a conventional CLC process, a metal oxide is circulated between two reactors in which they undergo changes from an oxidized form in the air reactor to a reduced form in the fuel reactor. In the air reactor, oxygen-depleted particles are exposed to a flow of air in which they are oxidized with O_2 according to Reaction (1):

$$O_2(g) + 2\,Me_xO_{y-1} \leftrightarrow 2\,Me_xO_y \quad (1)$$

The oxidized particles are then transported to the fuel reactor in which a fuel is used to reduce the particles with the formation of CO_2 and H_2O [Reaction (2)]:

$$(2n+m)\,Me_xO_y + C_nH_{2m} \leftrightarrow (2n+m)\,Me_xO_{y-1} + m\,H_2O + n\,CO_2 \quad (2)$$

Reduced particles are transferred back to the air reactor for reoxidation according to Reaction (1), and the cycle begins anew. The sum of Reactions (1) and (2) is the combustion of fuel with O_2, and the net reaction enthalpy released is the same as that of conventional combustion. However, in this case, the fuel is oxidized without mixing with N_2 from the air. Therefore, the flue gas consists mainly of CO_2 and H_2O undiluted with N_2. CLC has several attractive features. Most importantly, as cooling the off-gases is all that is needed to obtain an almost-pure CO_2 stream, CLC offers an ideal technology for the generation of heat and power with inherent CO_2 sequestration. The most commonly proposed oxygen-carrier materials are oxides of Mn, Fe, Cu, and Ni.

[a] Prof. A.-M. Azad
Department of Chemical Engineering
University of Toledo
Toledo, OH 43606-3390 (USA)
E-mail: abdul-majeed.azad@utoledo.edu

[b] A. Hedayati, Prof. H. Leion
Department of Chemical and Biological Engineering
Chalmers University of Technology
412 96 Göteborg (Sweden)

[c] Prof. M. Rydén, Prof. T. Mattisson
Department of Energy and Environment
Division of Energy Technology
Chalmers University of Technology
412 96 Göteborg (Sweden)

One notable variant of the CLC concept is chemical-looping with oxygen uncoupling (CLOU). Here, an oxygen-carrier material with the propensity to release gas-phase O_2 directly into the fuel reactor is used. In this case, although the net reaction in each reactor vessel is identical to that of CLC, the fuel oxidation mechanism is different. In ordinary CLC, oxidation takes place mainly by gas–solid reaction. Consequently, if a solid fuel such as coal or biomass is used, it has to be gasified to be able to react with the oxygen carrier. In contrast, in CLOU, solid fuel can react directly with gas-phase O_2 released by the carrier and hence does not need gasification.

In the case of CLOU, O_2 is released from the carrier in the gas phase, which enables combustion [Reactions (3) and (4)].

$$2\,Me_xO_y \leftrightarrow 2\,Me_xO_{y-1}+O_2(g) \quad (3)$$

$$1/2\,(2n+m)\,O_2(g)+C_nH_{2m} \leftrightarrow m\,H_2O(g)+n\,CO_2(g) \quad (4)$$

The CLOU process is applicable for all types of fuel but perhaps it is most advantageous in use with solid fuels for which CLOU enables conversion without a prior gasification step. Figure 1 shows a schematic description of CLC and CLOU.

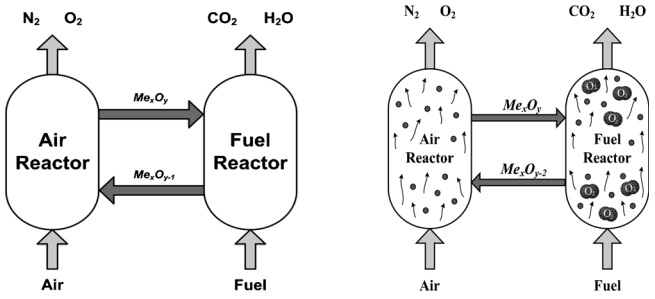

Figure 1. Process illustration for CLC (left) and CLOU (right).

Most often, chemical-looping reactors are designed as interconnected fluidized beds with oxygen-carrier particles used as the bed material. The particles are continuously transferred between the reactors.

The availability of feasible oxygen-carrier materials is one of the main challenges in the development of CLC and CLOU. Some of the prerequisites for the choice of oxygen carrier are adequate rates of oxidation and reduction, thermodynamic propensity (which allows a high conversion of the fuel into CO_2 and H_2O), and good resistance towards degradation, fragmentation, and agglomeration. The oxygen carrier should also preferably be inexpensive and environmentally benign. Other relevant criteria include a high melting point and high oxygen content,[7,8] which enable it to react according to Reactions (1) and (2) or Reactions (3) and (4) if it possesses CLOU properties.

CuO has been shown to have favorable properties such as high reactivity during reduction, which typically results in the full conversion of gaseous hydrocarbon fuels such as CH_4 or directly with coal.[9,10] Unlike the other most commonly proposed oxygen-carrier materials, the reaction of CuO with hydrocarbon fuels in the fuel reactor is exothermic, which could be advantageous from a heat balance point of view. Moreover, it is cheaper than some other commonly proposed materials such as nickel and cobalt oxides and its use is associated with fewer environmental problems. The use of CuO in CLC has been examined by several research groups. Gayán et al.[11] investigated the effect of different support materials on the behavior of CuO-based oxygen carriers. Chuang et al.[12] systematically investigated CuO–Al_2O_3 particles synthesized in three different ways and concluded that particles made by co-precipitation showed the best operational behavior. According to the work by de Diego et al.[13] and Forero et al.,[14] a 10 kW_{th} chemical-looping reactor was designed and operated for 100 h with CH_4 as the fuel and with 40 h with syngas as the fuel for CuO–Al_2O_3 particles prepared by impregnation.

Mn oxides are nontoxic, inexpensive, and have favorable thermodynamic properties. However, relatively few studies deal with the use of Mn-based oxygen carriers in CLC. These typically deal with composite particles of Mn oxides supported on alumina, magnesia, silica, titania, pure and stabilized zirconia, or magnesium aluminate.[15–17] However, Mn_3O_4 is prone to react with support materials (Al_2O_3, SiO_2, and TiO_2). Johansson et al.[18] investigated Mn_3O_4 supported on calcia-, magnesia-, and ceria-stabilized ZrO_2 and reported good performance during reduction with CH_4. Here, some materials showed a combination of high reactivity with the fuel, reasonable mechanical strength, and little or no tendency for defluidization. The magnesia-stabilized ZrO_2 support exhibited the best properties in terms of reactivity and stability, and its stable performance in a small continuously operated reactor for 70 h has been reported.[19]

The capability of Mn to participate effectively in a host of catalytic redox reactions is a result of multiplicity of oxidation states, which vary among +2, +2.67, +3, and +4 in MnO, Mn_3O_4, Mn_2O_3, and MnO_2, respectively. Among these, the phase relationship between Mn_2O_3 and Mn_3O_4 is of particular interest for CLC. At atmospheric pressure, stoichiometric Mn_2O_3 (with an atom fraction Mn/O of 0.4:0.6) is thermodynamically stable in air at temperatures below 900 °C.[20] At higher temperatures it decomposes into Mn_3O_4 [Eq. (5)].

$$6\,Mn_2O_3 \rightarrow 4\,Mn_3O_4+O_2 \quad (5)$$

Even though the amount of O_2 released by the reaction in Reaction (5) on a mass basis (grams of O_2 released per gram of oxide) is only approximately 3 %, this is likely sufficient to provide all or most of the O_2 by CLOU in a well-designed CLC reactor, provided that the release rate of O_2 is sufficient to burn the added fuel.[17] Mn_2O_3 decomposes completely into Mn_3O_4 at temperatures above 820 °C in 5 % O_2.[21] Unfortunately, this phase transformation is not truly reversible at temperatures higher than 800 °C, and only the presence of Mn_3O_4 has been established in the regenerated sample.[17] No

studies of pure Mn-oxide systems for CLC have reported any CLOU effects. This is likely a result of the rather low temperature range for the release of an appreciable amount of O_2 for this oxide pair, which results in slow reaction kinetics. On the other hand, several Mn-bearing systems such as Fe–Mn mixed oxides[22,23] and calcium manganate[24,25] have provided better results than those based on the Mn_2O_3–Mn_3O_4 couple.

In light of the inherent CLOU properties of the individual oxides in the Mn–O and Cu–O binaries,[26,27] it is interesting to explore the possibility of the same in the Mn–Cu–O ternary system with the goal to improve the performance and overcome the disadvantages of the individual parent oxides Mn_2O_3 and CuO, that is, unfavorable thermodynamics and kinetics for Mn_2O_3 and problems related to stability and agglomeration for CuO.[28] The rationale for this investigation also originates from the fact that amorphous hopcalite ($CuMn_2O_4$) has been used extensively as a potent catalyst for the oxidation of CO to CO_2 near room temperature and for the combustion of volatile organic carbons (VOCs) in the range of 200–500 °C by way of the facile redox equilibrium: $Cu^{2+}+Mn^{3+}\leftrightarrow Cu^{1+}+Mn^{4+}$ at specific sites.[29–33] Heating at approximately 350 °C leads to catalytic deactivation through crystallization of $CuMn_2O_4$ along with the formation of $CuMnO_2$ and Mn_3O_4 [Eq. (6)].

$$2\,CuMn_2O_4 \rightarrow 2\,CuMnO_2+Mn_3O_4+O_2 \quad (6)$$

Even the reduced formulations have been found to be active catalysts for the synthesis of methanol from H_2–CO–CO_2 mixtures.[34]

In this study, we report the performance of oxygen-carrier particles made from a mixture that consists of CuO (30.8 wt%) and Mn_2O_3 (69.2 wt%) (equivalent to a 1:1 molar ratio). The particles were synthesized by extrusion of intimately mixed powders, calcined at 950 °C for 6–12 h, and were examined as oxygen-carrier materials for CLC using CH_4 as fuel.

Results and Discussion

Evidence of CLOU propensity

To qualify as a prospective CLOU material, the solid oxygen-carrier particles must release gas-phase O_2 in the fuel reactor or even in an inert background. This requires the carrier to decompose to a reduced state as per Reaction (3). As a result of the favorable thermodynamic equilibria, both copper oxide (CuO–Cu_2O) and manganese oxide (Mn_2O_3–Mn_3O_4) are capable of releasing O_2 to a significant extent at temperatures higher than 700 °C.[4] Therefore, both these oxides are potential CLOU materials.

The samples calcined for 6 h at 950 °C will be hereafter designated as COMO1 and those calcined for 12 h as COMO2. No unreacted CuO or Mn_2O_3 was detected in the fresh COMO1 and COMO2 samples. However, the CLOU effect was clearly seen at 800 and 850 °C for both COMO1 and COMO2. The O_2-release characteristics of the particles during N_2 purging at these two temperatures is shown in Figure 2.

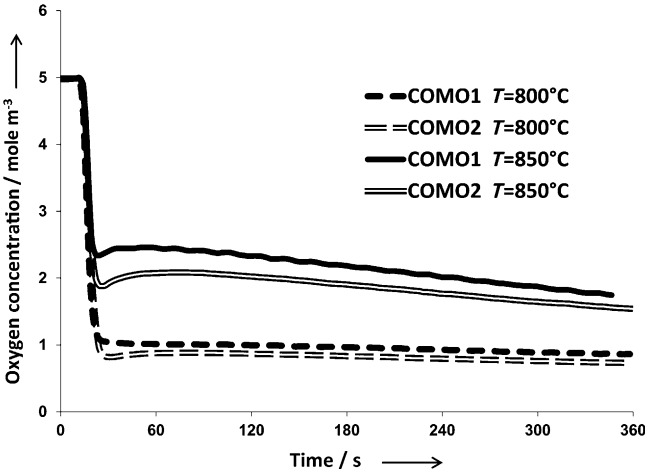

Figure 2. O_2 release profiles for the oxygen-carrier particles during fluidization with inert N_2 for 360 s.

The concentration of O_2 released after 360 s of fluidization using N_2 at 800 °C is approximately 0.8%; this is of interest as such a significant CLOU effect has not been seen at such low temperatures. Theoretically, there should be no major obstacle to perform a CLC process at 800 °C, provided that the reaction rates are sufficient, which may be the case for CuO. However, the rather high concentration of O_2 seen at this low temperature is significant, and we do not believe has been observed in previous studies. Accordingly, the O_2 concentrations in Figure 2 are considerably higher than the equilibrium O_2 concentrations for CuO.[35] With regard to O_2 analysis, there is not likely to be any interference with other gaseous species of relevance as the analytical method for each species is different: a paramagnetic method is used for the O_2 measurement and IR spectroscopy for CO_2, CO, and CH_4.

Although the equilibrium concentrations are higher for the Mn_2O_3-Mn_3O_4 transition, the oxidation of Mn_3O_4 is very slow at these temperatures for pure manganese oxides supported on inert carriers.[17] As expected, both COMO series release more O_2 in the gas phase at 850 °C than at 800 °C. In general, the CLOU behavior is very similar, though a slightly lower amount of O_2 is released from COMO2. However, the O_2 concentration decreases only slightly as a function of time, which suggests that the O_2-release rate is governed by equilibrium constraints. This will not be the case if the fuel is added to the reactor as the fuel will immediately react with the released O_2, which thereby removes any thermodynamic barriers for the overall fuel oxidation reaction. There is also a small increase in the crushing strength, see Table 1, which supports the fact that a longer soak time hardened the particles.

As no pure CuO or Mn_2O_3 was detected in the samples, the O_2 partial pressure is expected to be different in the two

Table 1. Composition and physical characteristics of the oxygen carriers investigated in this work.

Oxygen carrier	Composition [wt/wt]	ID	Calcination history	Size range [μm]	Crushing strength [N]	Bulk density [kg m^{-3}][a]
CuO–Mn_2O_3	31:69	COMO1	950 °C, 6 h	180–250	1.1 ± 0.2	1440
CuO–Mn_2O_3	31:69	COMO2	950 °C, 12 h	180–250	1.3 ± 0.2	2300

[a] Calculated by determining the mass of 5 mL of carrier particles in the size range of 125–180 μm.

COMO systems. Although no effort was made to determine the equilibrium value of O_2 in the $Cu_xMn_{3-x}O_4$ spinel, it is nevertheless highly relevant for the CLC process. The O_2 concentration obtained with the $Cu_xMn_{3-x}O_4$ spinel system is greater than that of carriers based on pure CuO. This means that the rates of O_2 release are also higher, which would clearly be an advantage with respect to fuel conversion in the fuel reactor.

Phase analysis, reactivity, and reaction pathways

The diffraction peaks of the extruded and dried COMO1 and COMO2 are shown in Figure 3a and b. Two spinel phases, [$Cu_3Mn_3O_8$ ($Cu_{1.5}Mn_{1.5}O_4$) and $Cu_{0.1}Mn_{2.9}O_4$], were identified in the XRD patterns of COMO1 and COMO2. No peaks that belong to unreacted tenorite (CuO), bixbyite (Mn_2O_3), or hausmannite (Mn_3O_4) were detected, which signifies that the reaction between CuO and Mn_2O_3 (or Mn_3O_4) was quantitative and was complete in a single firing at 950 °C. Moreover, $Cu_3Mn_3O_8$ appears to be the dominant phase, whereas $Cu_{0.1}Mn_{2.9}O_4$ is the minor component.

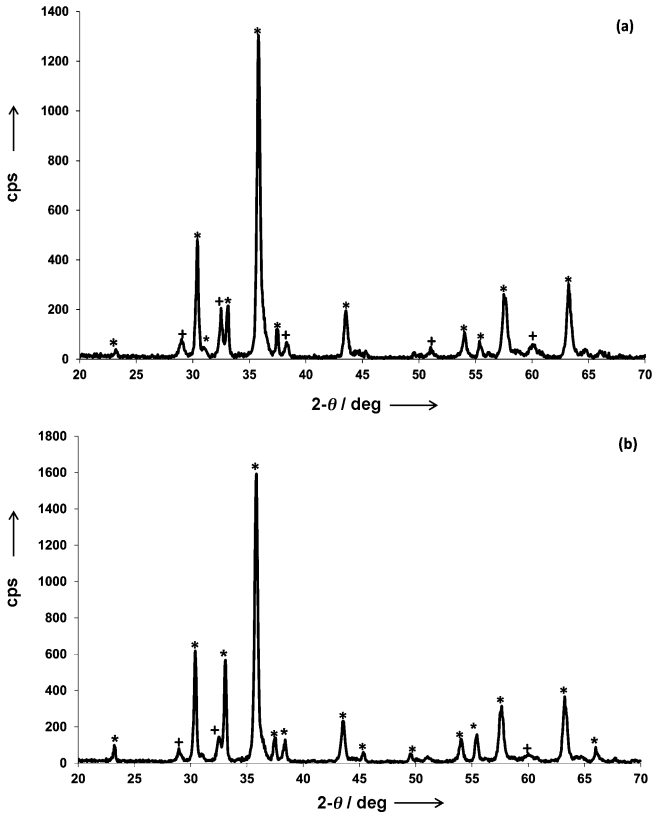

Figure 3. XRD patterns of as-prepared (a) COMO1 and (b) COMO2. $Cu_3Mn_3O_8$ (*), $Cu_{0.1}Mn_{2.9}O_4$ (+).

This is in complete conformity with previous studies on Cu–Mn–O, which have consistently reported that the solid-state reaction between Cu and Mn oxides at high temperatures (850–1100 °C) invariably leads to the formation of Cu-substituted hausmannite-type spinel phases of the general formula $Cu_xMn_{3-x}O_4$ in which x is defined as the mole fraction given as $x = 3\,Cu/(Cu+Mn)$.[36–39]

In light of this, we envisage the following reaction schemes for the formation of spinels with $x = 0.1$ and 1.5, assuming the interaction between CuO and bixbyite (Mn_2O_3) in one case and between CuO and hausmannite (Mn_3O_4) in the other (with Cu/Mn = 1:2):

$$2.8\,CuO + 2.8\,Mn_2O_3 \rightarrow 1.8\,Cu_{1.5}Mn_{1.5}O_4 + Cu_{0.1}Mn_{2.9}O_4 \quad (7a)$$

$$2.8\,CuO + 5.6/3\,Mn_3O_4 + 0.466\,O_2 \rightarrow 1.8\,Cu_{1.5}Mn_{1.5}O_4 + Cu_{0.1}Mn_{2.9}O_4 \quad (7b)$$

This reaction pathway is well corroborated by the systematic study made by Driessens and Rieck.[37]

To evaluate their reactivity and reproducibility, the oxygen carriers were subjected to successive reduction and oxidation cycles at 800 and 850 °C. Three redox cycles were performed using pure CH_4 as the fuel and a 5 % O_2–N_2 mixture as the oxidant with an inert run of high purity N_2 in between. Tests at temperatures higher than 850 °C were not conducted because of the possibility of defluidization and irreversible reduction. The gas yield as a function of the conversion of COMO1 and COMO2 for the third reduction cycle is shown in Figure 4.

The temperature dependence of the reactivity of the particles is evident; a much higher gas yield is obtained at 850 °C than at 800 °C. Similar to the O_2-release behavior seen in Figure 2, the reactivity of COMO1 is higher than that of COMO2 at both test temperatures. COMO1 shows superior behavior with a stable gas yield above 0.9 during the entire reduction period at 850 °C. Notably, the reactivity of the particles was not affected during successive redox cycles. The results of three successive reduction cycles using CH_4 for COMO1 at 850 °C are presented in Figure 5 as demonstrative evidence of the reproducibility of these oxygen carriers.

Another interesting observation from Figure 4 is the increasing trend in the gas-yield profile of COMO2. This could be a result of slow activation of the particles in the early stage of their reaction with CH_4. As the reduction progresses, the porosity of the particles increases, which results in a higher surface area and makes the reaction of the fuel with the oxygen carrier more effective. On the other hand, the temperature increase during the reaction with CH_4 (caused by the exothermicity of the reaction) could be another

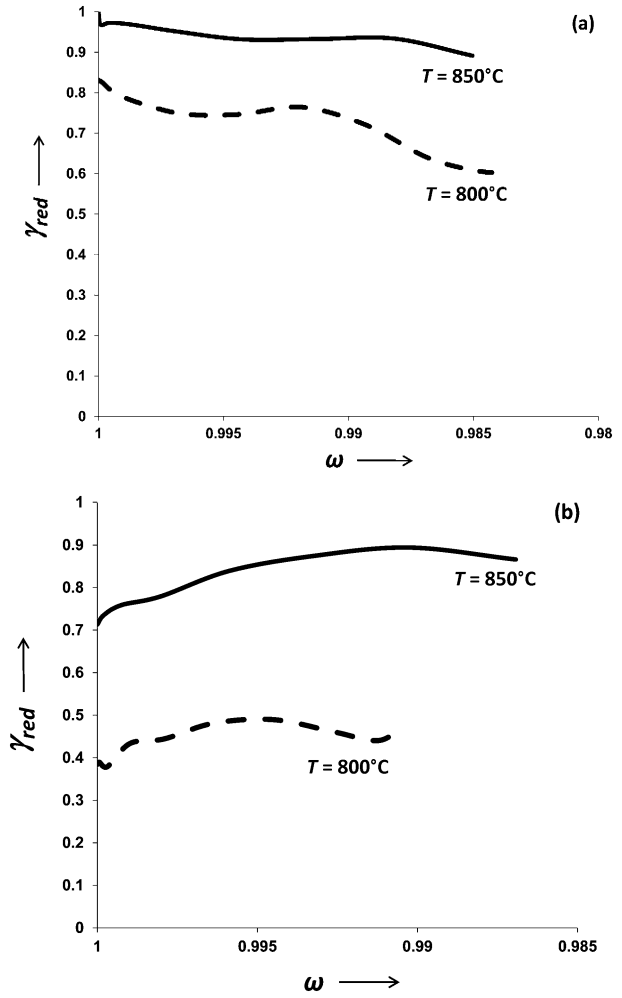

Figure 4. Gas yield (γ_{red}) as a function of conversion (ω) for the third cycle of (a) COMO1 and (b) COMO2 at 800 and 850 °C using CH_4 as a fuel.

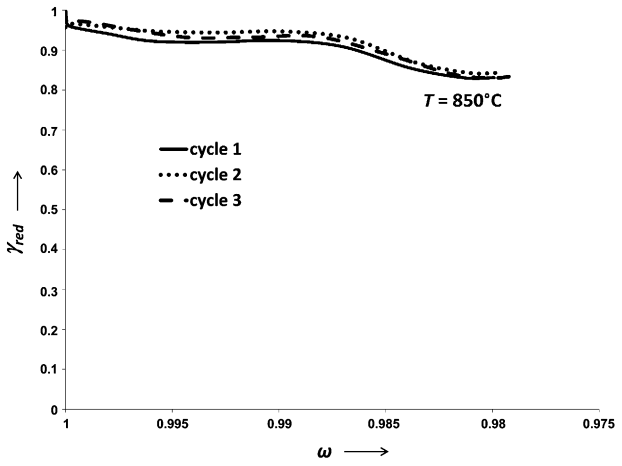

Figure 5. Gas yield as a function of conversion for three successive reduction cycles of COMO1 at 850 °C using CH_4 as a fuel.

reason for the enhancement of the oxygen release and higher fuel conversion.

The correlation between O_2 concentration and the concomitant temperature increase is shown in Figure 6 for the reduction phase at 850 °C using COMO2 and CH_4 as the

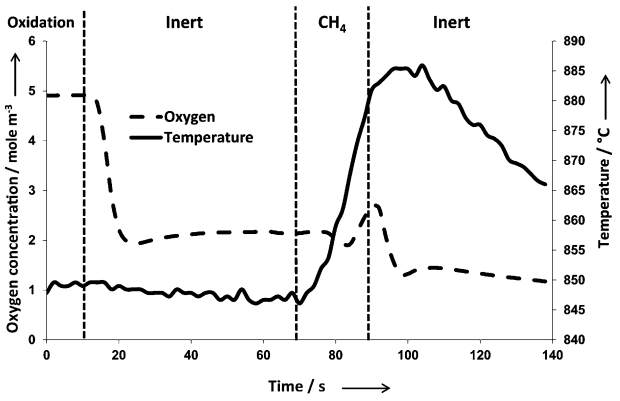

Figure 6. O_2 concentration and temperature profiles for COMO2 during reduction with CH_4 at 850 °C.

fuel. The vertical dashed lines signify the time intervals during which different gases were streamed. Pure N_2 was purged as an inert sweep gas for 60 s immediately before and after the reduction period.

As the oxygen carriers were reduced, the temperature increased by approximately 35 °C, which triggered greater oxygen release. Moreover, with reduction in progress, the O_2 concentration did not approach zero, which means that there was O_2 in the exit stream together with unreacted fuel. Thus, taking into account the observed temperature increase caused by the exothermic reduction, the increase in gas yield shown in Figure 5 is reasonable.

However, it should be emphasized that the rather high concentration of O_2 could be an artifact of how the gas analysis was performed. Generally, the CH_4 added to the fuel reactor is converted into CO_2 and H_2O. O_2 is released so that thermodynamic equilibrium is achieved, which is based on the partial pressure of O_2 in the wet flue gas. Steam is condensed and O_2 is measured in the dry flue-gas stream. As the stoichiometric oxidation of 1 mol of CH_4 produces 1 mol of CO_2 and 2 mol of H_2O, three times as much O_2 (dry basis) is expected at equilibrium when CH_4 is used as the fluidizing media in the reactor than if N_2 is used.

The time-dependent concentration profiles for various gases for the third reduction cycle of COMO2 at 850 °C are presented in Figure 7. The full conversion of fuel is dependent both on the nature of the fuel and the reactivity of the oxygen carrier. In the case of COMO1 and COMO2, there is a substantial CLOU effect. Thus, it could be argued that although most of the fuel is converted by gas-phase reaction with O_2 released from the carrier, not all fuel is converted, which is why O_2 and CH_4 were detected in the exhaust of the fuel reactor. The simultaneous presence of CH_4 and O_2 in the exit stream can be explained in two ways. First, the reaction temperature reached a maximum of 885 °C, which is lower than that usually observed if copper oxide (test temperature: 925 °C) or manganese oxide (test temperature: 950 °C) are used in the same set-up.[39] Hence, in light of the observed temperature dependence of the gas yield, it is reasonable to expect a lower fuel conversion at 800 and 850 °C. Second, the simultaneous presence of CH_4 and O_2 could be

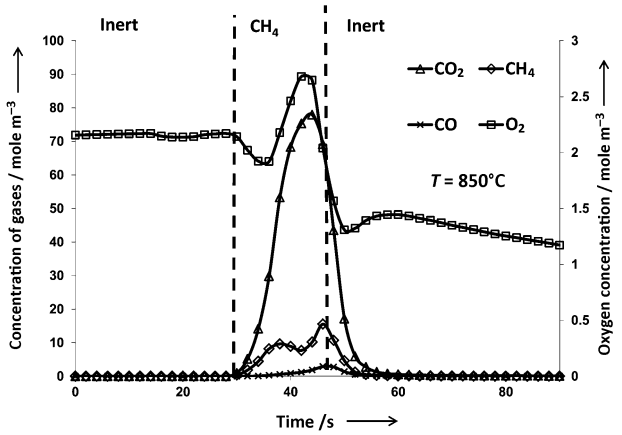

Figure 7. Time-dependent concentration profile during a typical reduction of COMO2 at 850 °C.

expected because the hot zone in the reactor in this study was rather short and the oxidation of CH_4 to CO_2 and H_2O is somewhat more complex than that of simpler fuels such as syngas.

The XRD signatures of COMO1 and COMO2 after reduction by CH_4 at 850 °C are shown in Figure 8. Evidently,

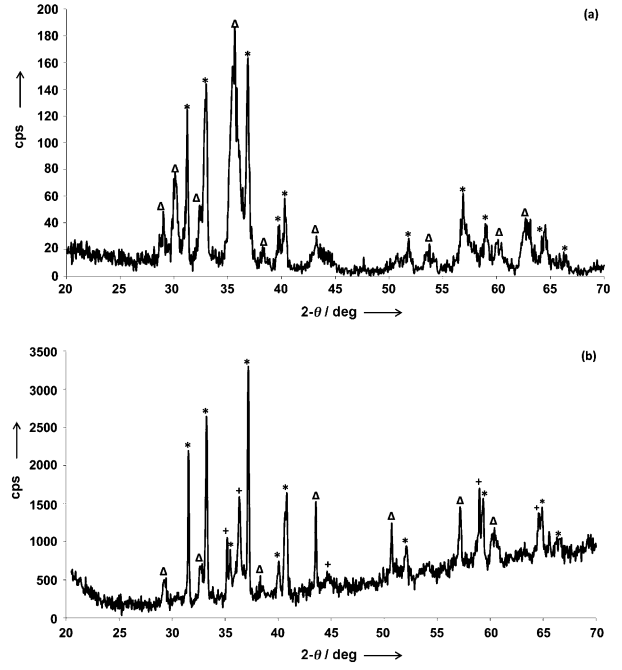

Figure 8. XRD patterns of CH_4-reduced (a) COMO1 and (b) COMO2. $CuMnO_2$ (*), $CuMn_2O_4$ (+), Mn_3O_4 (Δ).

the spinels present in the fresh samples were reduced in the fuel reactor to $CuMnO_2$. Thus, the likely reaction pathway in the two cases can be represented as:

$$Cu_3Mn_3O_8 + Cu_{0.1}Mn_{2.9}O_4 \rightarrow 3.1\,CuMnO_2 + 2.8/3\,Mn_3O_4 + 1.034\,O_2 \quad (8)$$

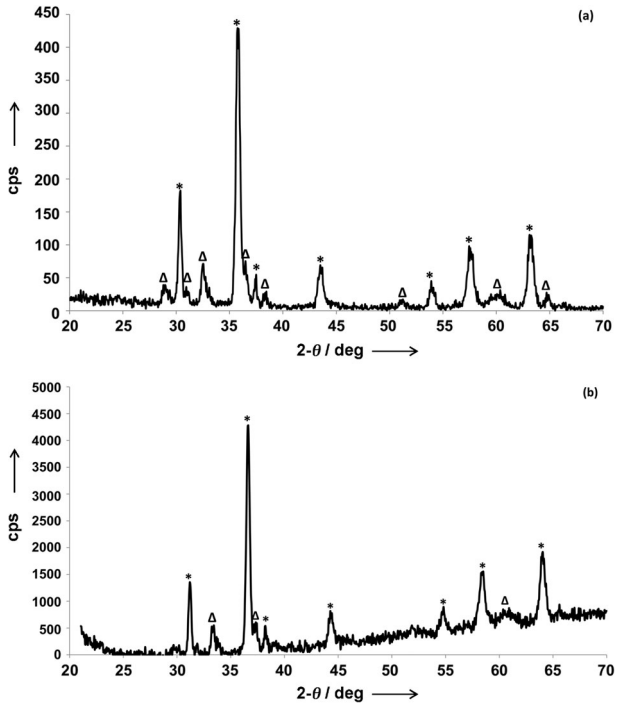

Figure 9. XRD patterns of (a) COMO1 and (b) COMO2 reoxidized (after reduction by CH_4) by a stream of 5% O_2–N_2 at 850 °C. $Cu_{1.2}Mn_{1.8}O_8$ (*), Mn_3O_4 (Δ).

The XRD signatures collected after subjecting the reduced COMO1 and COMO2 particles to oxidation in 5% O_2–N_2 at 850 °C are shown in Figure 9. The XRD signatures of the regenerated particles in the two cases are quite similar, which suggests that the reaction sequence of oxidation in the two cases is identical. Upon reoxidation, only one spinel ($Cu_{1.2}Mn_{1.8}O_4$) is regenerated.

In light of this, the regenerative mechanism could be represented as:

$$6\,CuMnO_2 + Mn_3O_4 + 2\,O_2 \rightarrow 5\,Cu_{1.2}Mn_{1.8}O_4 \quad (9)$$

From reactions (8) and (9) it can be concluded that not all Mn_3O_4 produced during the first reduction with the fuel is included in the reoxidized sample. Furthermore, at the temperatures and O_2 partial pressures used in this study, oxidation to Mn_2O_3 is not possible, which means that the reoxidized samples will still contain small amounts of Mn_3O_4 (Figure 9).

Fluidization and agglomeration characteristics

The fluidization of the oxygen carriers during the experiments was monitored by pressure measurements over the bed. Sudden and very steep temperature increases during reduction cycles can result in defluidization of the reduced oxygen carriers. No agglomeration was observed even after reduction by CH_4.

Near the exit of the reactor, the gas passes through a piece of quartz wool, which is used to ensure that no dust formed in the reactor enters the gas sampling system. The results of the experiments conducted with the COMO series showed the apparent stability of particles against degradation; no dust was captured in the quartz wool even after more than 10 h of fluidization. These characteristics suggest that COMO particles are resistant to physical and chemical attrition. The gas velocity used in these experiments is lower than the conditions that would be suitable for practical operation. Still, the apparent lack of dust formation is very positive.

Thermodynamic analysis of the Cu–Mn–O system relevant to CLC reactions

Cu–Mn–O is a three-component system, which, according to Gibbs' phase rule, requires five variables to define the system completely. For a meaningful depiction of the phase relationships, the number of variables can be reduced by writing the composition as a ratio rather than an absolute value. Moreover, if we consider only condensed phases at ambient pressure (1 bar), the system can be described by only three variables: the mole fraction, temperature (T), and the oxygen partial pressure (pO_2). The mole fraction is defined in terms of Cu as $x = 3\,\mathrm{Cu}/(\mathrm{Cu}+\mathrm{Mn})$, and thus, one could construct a T–x (at a constant pO_2) or a pO_2–x (at constant temperature) diagram.[36] On the basis of systematic phase evolution from the XRD signatures of the fresh, reduced, and regenerated oxygen-carrier particles, it can be concluded that the spinel in the Cu–Mn–O system is best represented as $Cu_xMn_{3-x}O_4$. Moreover, each of these spinels reduces to $CuMnO_2$ in the presence of CH_4.

Therefore, in the fresh and oxidized samples, the phases oscillate between Mn_3O_4 ($x=0$) and $Cu_{1.5}Mn_{1.5}O_4$ ($x=1.5$; Table 2). We can also define a parameter y akin to x as the mole fraction of CuO; the computed values of y that correspond to x are also shown in Table 2.

Table 2. Phase relationships in the Cu–Mn–O spinel at different values of x.

$x = 3 \cdot \frac{\mathrm{Cu}}{(\mathrm{Cu}+\mathrm{Mn})}$	$Cu_xMn_{3-x}O_4$	$y = \frac{x_{CuO}}{\left(x_{CuO}+x_{Mn_3O_4}\right)}$ [c]
0	Mn_3O_4	0
0.1	$Cu_{0.1}Mn_{2.9}O_4$	0.093
0.5	$Cu_{0.5}Mn_{2.5}O_4$ [a]	0.375
1.0	$CuMn_2O_4$	0.600
1.2	$Cu_{1.2}Mn_{1.8}O_4$	0.667
1.5	$Cu_{1.5}Mn_{1.5}O_4$ [b]	0.75

[a] $CuMn_5O_8$. [b] $Cu_3Mn_3O_8$. [c] The parameter y was derived by writing each $Cu_xMn_{3-x}O_4$ composition as $CuO{\cdot}Mn_3O_4$.

Using the phases that evolve from the processing history employed in this investigation (including the high pO_2 in the air, fuel, and oxidizing environment) an isothermal contour of the Cu–Mn–O ternary system was constructed. A 2D planar section of this contour is shown in Figure 10 (left). As seen from Reactions (7)–(9), various oxidized (spinel) compositions are connected to the reduced form crednerite ($CuMnO_2$) via haussmanite (Mn_3O_4). This is shown in Figure 10 (right) as a cross-sectional slice.

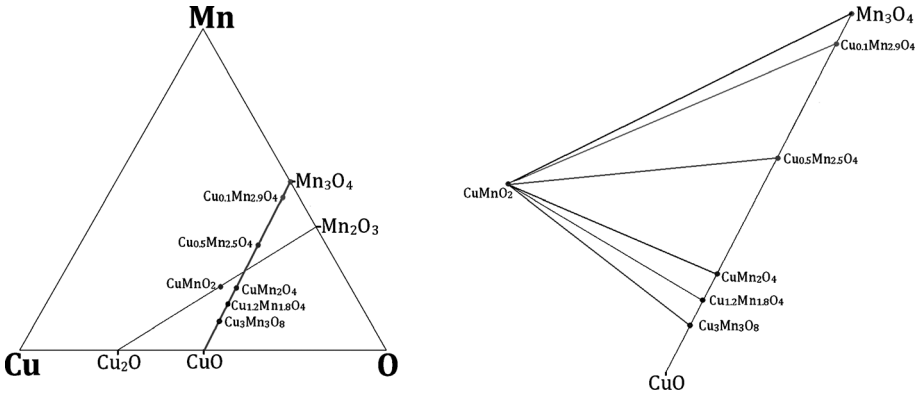

Figure 10. Phase relationships in the Cu–Mn–O system relevant to the redox cycle in CLC (validity range: 850–950 °C and 1 atm total pressure).

This representation delineates the phase relationship relevant to the redox cycle of the CLC process that operates in the Cu–Mn–O system in the temperature range from 850–950 °C. Thus, it can be concluded that the spinels in the Cu–Mn–O systems are effective oxygen carriers for CLC applications with envisaged CLOU properties.

Comparison with the Cu-Al-O system

It is relevant to examine some interesting resemblances and unique differences between the Cu–Al–O and Cu–Mn–O ternary systems, both of which are relevant for CLC and CLOU.

First, in the case of the Cu–Al–O system, there are no oxygen-releasing species along the Al–O line. On the contrary, there are four stoichiometric compounds in the Cu–Mn–O system along the Mn–O line: MnO, Mn_3O_4, Mn_2O_3, and MnO_2. These are related by three equilibria that involve O_2: MnO–Mn_3O_4, Mn_3O_4–Mn_2O_3, and Mn_2O_3–MnO_2. However, from a practical point of view, only the Mn_2O_3–Mn_3O_4 phase field is relevant for O_2 release in the CLOU process.

Theoretically, there are two modes of gas-phase O_2 release from individual oxides by virtue of the CuO–Cu_2O and Mn_2O_3–Mn_3O_4 equilibria in Cu–Mn–O. However, there was no evidence of free CuO or Cu_2O in the XRD signatures of the fresh, reduced, or oxidized specimens. This shows that CuO was fully consumed in the formation of the substituted spinels.

Second, there is only one stoichiometric spinel ($CuAl_2O_4$) in the CuO–Al_2O_3 system, which is related to the reduced

delafossite-structured compound, $CuAlO_2$. Cu exists as Cu^{II} and Cu^{I} species in Cu_2AlO_4 and $CuAlO_2$, respectively. On the other hand, a series of Cu-substituted spinels ($Cu_xMn_{3-x}O_4$) exist in the $CuO–Mn_2O_3$ pseudobinary, only one of which ($CuMn_2O_4$ with $x=1$) is isostructural with $CuAl_2O_4$. However, in light of the XRD analyses discussed above, all of the ternary phases in the $Cu_xMn_{3-x}O_4$ series are related to the reduced form (i.e., crednerite, $CuMnO_2$) and the terminal binary oxide (Mn_3O_4) by releasing gas-phase O_2. The spinel phases in the 1:1 molar mixture of CuO and Mn_2O_3 are also formed at 950 °C, as was the case with a 1:1 CuO and Al_2O_3 molar mixture.[40]

Similarly, as the oxidation of delafossite ($CuAlO_2$) regenerates the spinel $CuAl_2O_4$, the crednerite ($CuMnO_2$) phase upon oxidation regenerates the spinel $Cu_xMn_{3-x}O_4$, albeit by a much simpler reaction scheme.

The facile regeneration of the active phase $Cu_xMn_{3-x}O_4$ from the reduced crednerite ($CuMnO_2$) over several redox cycles indicates that, unlike delafossite, the reaction of crednerite is kinetically fast.

Finally, as is the case with the $CuAl_2O_4$ spinel in the $CuO–Al_2O_3$ system,[41,42] the compounds in the $CuO–Mn_2O_3$ series formed by the solid-state reaction between CuO and Mn_2O_3 are promising CLC materials; they are capable of acting as CLOU materials as well, supported by the reaction schemes elucidated in Reactions (8) and (9). An investigation of their CLOU properties is currently underway.

Conclusions

This work was carried out to explore: i) the cooperative synergism between the two metal oxides CuO and Mn_3O_4 if used together and ii) to accentuate the performance of one oxygen carrier in the presence of another. Equimolar mixtures of CuO and Mn_2O_3 were extruded, calcined at 950 °C for 6 or 12 h, and sieved to prepare the mixed oxygen-carrier particles. Experiments with CH_4 as the fuel demonstrated that the combined oxide, which forms a $Cu_xMn_{3-x}O_4$ spinel in the Cu–Mn–O system, performed excellently in a highly reproducible manner with no evidence of material or physical degradation over repeated use in several redox cycles. Detailed and systematic phase analyses were performed in light of different coexisting phases identified in the fresh, reduced, and regenerated carriers. Based on this, the underlying mechanism of the mixed Cu–Mn–O system was elucidated. The oxidized $Cu_xMn_{3-x}O_4$ phases were reduced by CH_4 to copper(I) manganate ($CuMnO_2$; crednerite) and Mn_3O_4 with concomitant release of O_2. $CuMnO_2$ demonstrated a faster reaction rate for its oxidation to the parent copper manganate ($Cu_xMn_{3-x}O_4$) phase compared to its delafossite analog $CuAlO_2$ in the $CuO–Al_2O_3$ pseudobinary in similar experiments.[41] This suggests swift and reproducible oscillation of spinel $Cu_xMn_{3-x}O_4$ in the freshly prepared particles, $CuMnO_2$ and Mn_3O_4 in the reducing environment, and $Cu_xMn_{3-x}O_4$ and Mn_3O_4 in the oxidizing environment.

We propose that the various oxides in the spinel $Cu_xMn_{3-x}O_4$ system under the oxidizing conditions are related to crednerite ($CuMnO_2$) in the fuel reactor through haussmanite (Mn_3O_4) and O_2 in a facile manner. The reaction pathway includes the release of O_2 in a reducing atmosphere. This characteristic makes the system a promising CLOU material for solid fuels such as coal and biomass. The oxygen-carrier particles performed well without a support material over several redox cycles, and their oxidation was faster than that of $CuAlO_2$ in the $CuO–Al_2O_3$ system. It is concluded that the COMO materials are promising as oxygen-carrier materials for CLC as well as for CLOU. Further work is needed to verify the long-term stability and physical characteristics such as degradation resistance.

Experimental Procedure

Fabrication of oxygen-carrier particles

The oxygen-carrier particles were manufactured in two stages. First, CuO (97 %) and Mn_2O_3 (99 %) powders (Alfa–Aesar, average grain size ~46 μm, 325 mesh) were mixed in a 30.8:69.2 weight ratio in three batches of 125 g each.

Each solid mixture (125 g) and water (400 mL) was transferred to a 1 L pear-shaped distillation flask, which was placed in a temperature-programmable 20 L water bath. The aqueous slurry was thoroughly mixed and homogenized by using a Büchi R-110 rotary evaporator unit that was interfaced with a Büchi vacuum pump (V-710), a programmable Büchi vacuum controller (V-850), and a Büchi recirculating chiller (F-105). The rotary evaporator was operated according to the 20/40/60 rule, the cooling water in the chiller was at 20 °C, the boiling temperature of the water used as the solvent at reduced pressure was 40 °C, and the bath temperature was 60 °C. The rotary-evaporator operation was initiated at a relatively low vacuum level and the vacuum level was increased gradually as the evaporation continued. This pressure modulation varied from system to system. The duration of the evaporation was approximately 2 h for each 125 g batch, which ensured thorough mixing and uniform homogenization of the powders. A concentrated and viscous (albeit smooth-flowing) slurry was obtained after approximately two-thirds of the water had been removed by evaporation. The slurry was poured into a shallow Pyrex pan and dried at 150 °C in an air oven overnight. The dried, soft, cakey mass was then crushed and ground to a homogenous powder for each batch. Finally, all the batches were mixed and homogenized again.

The resulting powder was used for extrusion as follows. The powder (340 g) was mixed manually in a wide-mouthed plastic container with poly(vinyl alcohol) (20 g, Alfa–Aesar, average molecular weight of 25000) as a binding agent, soluble starch ($(C_6H_{10}O_5)_n$, 4 g, Merck) as an auxiliary binder, and LAROSTAT 519 (4 g, a quaternary ammonium salt that functions as antistatic agent, PPG Industries) to increase the flux properties of the mixture. Next, ammonium hydroxide (8 g, 1 M) as peptizing agent and water (64 g) were added. The somewhat wet mixture was then transferred to a food processor for mixing and homogenization. The ingredients were mixed mechanically, with intermittent stirring using a plastic spatula until a pliant and flexible dough of plasticity suitable for extrusion was obtained.

The dough was transferred to a hand-held single-screw extruder and squeezed to form individual strands. This process helped to avoid the fine dust formation that occurred if the powder was directly transferred to the food processor for mixing and also yielded optimum strands. This procedure was optimal to produce the

dough for reproducible extrusion. A more efficient mechanical mixer would be needed for larger batches.

The strands were collected on a stainless-steel sheet and dried in an air oven at 200–220 °C overnight. The dried extrudates were divided into two batches and transferred to high-density alumina crucibles. One batch was calcined in air for 6 h and the other for 12 h at 950 °C in a programmable muffle furnace using the temperature–time profile shown in Scheme 1.[34]

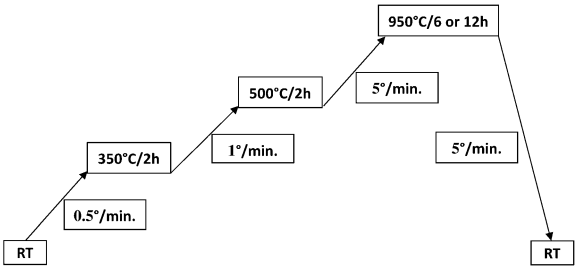

Scheme 1. Temperature–time profile used for the calcination of the extrudates.

The samples calcined for 6 h at 950 °C are designated as COMO 1 and those calcined for 12 h as COMO 2 (Table 1). The calcined extrudates were sieved through stainless-steel screens to yield particles in the range of 125–180 μm and 180–250 μm.

Particle characterization

The oxygen carriers fabricated and used in this study are listed in Table 1 together with their physical characteristics, such as the crushing strength and apparent density. Systematic phase analysis of the fresh, reduced, and oxidized particles was carried out by using XRD (Siemens, D5000 diffractometer) with CuK_α radiation. The crushing strength was measured for 30 individual particles by using a digital force gauge (Shimpo, FGN-5) as the force required to fracture the particles that were within the 180–250 μm size. An average of all 30 measurements was taken as the representative strength with a standard deviation of ±0.2 N.

Experimental set-up

The experiments were performed in a batch fluidized-bed reactor made of quartz, which was 870 mm long and had an inner diameter of 22 mm. A porous quartz plate was placed at a height of 370 mm from the bottom. The reactor temperature was measured by using chromel–alumel (type K) thermocouples sheathed in inconel-600 located approximately 5 mm below and 25 mm above the plate. Honeywell pressure transducers were used to measure the pressure drop over the bed of particles and the quartz plate at a frequency of 20 Hz. The pressure drop over the quartz plate was approximately constant for constant flows. By measuring the fluctuations in the pressure drop, it is possible to determine if the particles were fluidized or not, that is, defluidization would be noted from reduced pressure fluctuations. A schematic description of the experimental set-up used in this investigation is shown in Figure 11.

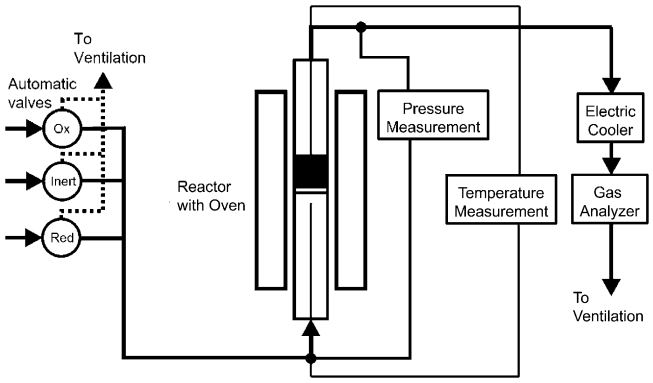

Figure 11. Schematic of the experimental set-up used in this investigation.

Test protocol

In a typical experiment, the oxygen-carrier particles (15 g) were placed onto the porous plate. The reactor was placed inside a vertically split furnace, and the experiment was initiated by heating the reactor to 800 °C. In some cases, tests were conducted at 850 °C. During heat-up, the oxygen-carrier particles were fluidized with a gas mix of 5 % O_2 and 95 % N_2 to ensure full oxidation of the particles prior to the experiments. The use of a 5 % O_2 mixture was aimed to be similar to the expected conditions at the air-reactor outlet in an industrial reactor and to obviate a large temperature increase during the exothermic oxidation.

When the desired temperature was reached, the experiment was initiated. To investigate the performance of the material, the particles were exposed to successive reduction and oxidation periods. Pure (100 %) CH_4 was used as a fuel for reduction. CH_4 was chosen as it is the main component of natural gas. Oxidation was performed with 5 % O_2 in N_2. To prevent the reducing and oxidizing gases from mixing, pure N_2 was injected for 60 s between every reduction and oxidation sequence. The experiments were performed at a u/u_{mf} (the ratio of the superficial gas velocity and the minimum fluidization velocity) of 3–5 for the reducing period and 7–12 for the inert and oxidizing periods as calculated from the correlations given by Kuuni and Levenspiel.[44] A particle sphericity of 0.8 was assumed in the calculations, and these values were calculated for the inlet flow to the reactor. During the reduction with CH_4, there was gas expansion caused by the reaction, which means that the actual velocities in the bed were considerably higher.

For the initial reactivity tests, the oxygen-carrier particles were exposed to fuel during the reduction cycles, and each cycle was repeated at least three times to assess the reproducibility and reliability of the process as well as the reversibility of the oxygen carriers. The reduction time for each material was calculated on the basis of the flow rate and the maximum amount of O_2 available in each case for the reaction with CH_4 and then adjusted accordingly. The oxidation time was sufficiently long to allow the complete regeneration of the carriers. The reactor was purged with N_2 for 60 s before and after the fuel cycles and after the full oxidation of the particles to examine their O_2 uncoupling behavior. A summary of the experimental variables used in this work is presented in Table 3.

The XRD patterns of the reduced and reoxidized particles were collected to establish the reaction scheme that the materials underwent in each environment.

Table 3. Test conditions employed to evaluate the oxygen carriers. All flows are normalized to 0 °C and 1 bar.

Test temp. [°C]	N_2		CH_4		5% O_2 in N_2	
	Flow rate [ml min^{-1}]	Duration [s]	Flow rate [ml min^{-1}]	Duration [s]	Flow rate [ml min^{-1}]	Duration
800	900	60	600	20	900	Until fully oxidized
850	900	60	600	20	900	Until fully oxidized
800	900	60	600	20	900	Until fully oxidized
850	900	60	600	20	900	Until fully oxidized

Data analysis

The gas stream exiting from the reactor was fed into a condenser to remove water, hence all measurements are on dry gases, the composition and flow rate of which was determined on a volumetric basis by using a Rosemount NGA-2000 analyzer, which measured the concentration of O_2, CO_2, CO, CH_4, and H_2 as well as the total volumetric gas flow.

The reactivity of a given oxygen carrier is quantified in terms of gas yield (γ_{red}) and is defined as the fraction of fully oxidized fuel divided by the amount of C-containing gases in the outlet stream, which in this work are CO_2, CO, and CH_4.

$$\gamma_{red} = \frac{x_{CO_2}}{x_{CH_4} + x_{CO_2} + x_{CO}} \tag{10}$$

Here x_i denotes the composition of the respective gas obtained from the measured concentration in the gas analyzer.

The theoretical O_2 capacity of a given oxygen carrier is defined in terms of the oxygen ratio (R_o) as the fraction of theoretical maximum mass change to the molecular mass of the carrier as follows:

$$R_O = \frac{m_{ox} - m_{red}}{m_{ox}} \tag{11}$$

in which m_{ox} and m_{red} are the masses of the oxygen carrier in the fully oxidized and reduced states, respectively. The mass-based conversion of the oxygen carrier (ω) is defined as:

$$\omega = \frac{m}{m_{ox}} \tag{12}$$

in which m is the actual mass of the carrier. Equations (13) and (14) were employed to calculate ω as a function of time during the reduction period from the measured concentrations of various gaseous species in the gas analyzer for CH_4 and syngas cycles, respectively:

$$\omega_i = \omega_{i-1} - \int_{t_0}^{t_1} \frac{\dot{n}_{out} M_O}{m_{ox}} \left(4 x_{CO_2} + 3 x_{CO} - x_{H_2}\right) dt \tag{13}$$

$$\omega_i = \omega_{i-1} - \int_{t_0}^{t_1} \frac{\dot{n}_{out} M_O}{m_{ox}} \left(2 x_{CO_2} + x_{CO} - x_{H_2}\right) dt \tag{14}$$

Here, ω_i is the instantaneous conversion at time i, ω_{i-1} is the conversion in the preceding instant, t_0 and t_1 are the initial and final time of the measurements, respectively, M_o is the molecular weight of oxygen, and $\dot{n}_{out}$ is the molar flow rate of the gas at the reactor outlet after water removal. The carrier is assumed to be fully (100%) oxidized prior to each reduction cycle for the calculation of ω.

Keywords: carbon dioxide · copper oxide · manganese oxide · redox chemistry · spinel phases

[1] *IPCC Fourth Assessment Report: Climate Change 2007 (AR4)*, Intergovernmental Panel on Climate Change, Switzerland.
[2] W. K. Lewis, E. R. Gilliland, W. P. Sweeney, *Chem. Eng. Prog.* **1951**, *47*, 251–256.
[3] M. M. Hossain, H. I. de Lasa, *Chem. Eng. Sci.* **2008**, *63*, 4433–4451.
[4] H. Fang, H. Li, Z. Zhao, *Int. J. Chem. Eng.* **2009**, 710515, 1–16.
[5] A. Lyngfelt, *Oil Gas Sci. Technol.–Rev IFP Energies Nouvelles* **2011**, *66*, 161–172.
[6] B. Moghtaderi, *Energy Fuels* **2012**, *26*, 15–40.
[7] E. Jerndal, T. Mattisson, A. Lyngfelt, *Chem. Eng. Res. Des.* **2006**, *84*, 795–806.
[8] T. Pröll, K. Mayer, J. Bolhàr-Nordenkampf, P. Kolbitsch, T. Mattisson, A. Lyngfelt, H. Hofbauer, *Energy Procedia* **2009**, *1*, 27–34.
[9] R. Siriwardane, H. Tian, G. Richards, T. Simonyi, J. Poston, *Energy Fuels* **2009**, *23*, 3885–3892.
[10] Y. Cao, B. Casenas, W.-P. Pan, *Energy Fuels* **2006**, *20*, 1845–1854.
[11] P. Gayán, C. R. Forero, A. Abad, L. F. de Diego, F. García-Labiano, J. Adánez, *Energy Fuels* **2011**, *25*, 1316–1326.
[12] S. Y. Chuang, J. S. Dennis, A. N. Hayhurst, S. A. Scott, *Combust. Flame* **2008**, *154*, 109–121.
[13] L. F. de Diego, F. García-Labiano, P. Gayán, J. Celaya, J. M. Palacios, J. Adánez, *Fuel* **2007**, *86*, 1036–1045.
[14] C. R. Forero, P. Gayán, L. F. de Diego, A. Abad, F. García-Labiano, J. Adánez, *Fuel Process. Technol.* **2009**, *90*, 1471–1479.
[15] J. Adánez, F. García-Labiano, L. F. de Diego, P. Gayán, J. Celaya, A. Abad, *Proceedings of the 7th International Conference on Greenhouse Gas Control Technologies (GHGT-7)*, Vancouver, Canada **2004**.
[16] Q. Zafar, T. Mattisson, B. Gevert, *Energy Fuels* **2006**, *20*, 34–44.
[17] Q. Zafar, A. Abad, T. Mattisson, B. Gevert, M. Strand, *Chem. Eng. Sci.* **2007**, *62*, 6556–6567.
[18] M. Johansson, T. Mattisson, A. Lyngfelt, *Chem. Eng. Res. Des.* **2006**, *84*, 807–818.
[19] A. Abad, T. Mattisson, A. Lyngfelt, M. Rydén, *Fuel* **2006**, *85*, 1174–1185.
[20] E. R. Stobbe, B. A. de Boer, J. W. Geus, *Catal. Today* **1999**, *47*, 161–167.
[21] W. B. White, S. M. Johnson, G. B. Dantzig, *J. Chem. Phys.* **1958**, *28*, 751–755.
[22] M. Rydén, A. Lyngfelt, T. Mattisson, *Energy Procedia* **2011**, *4*, 341–348.
[23] G. Azimi, H. Leion, T. Mattisson, A. Lyngfelt, *Energy Procedia* **2011**, *4*, 370–377.
[24] H. Leion, Y. Larring, E. Bakken, T. Mattisson, R. Bredesen, A. Lyngfelt, *Energy Fuels* **2009**, *23*, 5276–5283.
[25] M. Rydén, A. Lyngfelt, T. Mattisson, *Int. J. Greenhouse Gas Control* **2011**, *5*, 356–366.
[26] T. Mattisson, H. Leion, A. Lyngfelt, *Fuel* **2009**, *88*, 683–690.
[27] H. Leion, T. Mattisson, A. Lyngfelt, *Energy Procedia* **2009**, *1*, 447–453.
[28] P. Porta, G. Moretti, M. Musicanti, A. Nardella, *Catal. Today* **1991**, *9*, 211–218.
[29] L. S. Puckhaber, H. Cheung, D. L. Cocke, A. Clearfield, *Solid State Ionics* **1989**, *32/33*, 206–213.
[30] G. M. Schwab, S. B. Kanungo, *Z. Phys. Chem.* **1977**, *107*, 109–120.
[31] S. Vepřek, D. L. Cocke, S. Kehl, H. R. Oswald, *J. Catal.* **1986**, *100*, 250–263.

[32] M. Haruta, T. Kobayashi, H. Sano, N. Yamada, *Chem. Lett.* **1987**, *16*, 405–408.
[33] Z. R. Tang, S. A. Kondrat, C. Dickinson, J. K. Bartley, A. F. Carley, S. H. Taylor, T. E. Davies, M. Allix, M. J. Rosseinsky, J. B. Claridge, Z. Xu, S. Romani, M. J. Crudace, G. J. Hutchings, *Catal. Sci. Technol.* **2011**, *1*, 740–776.
[34] A. Hedayati, A.-M. Azad, M. Rydén, H. Leion, T. Mattisson, *Ind. Eng. Chem. Res.* **2012**, *51*, 12796–12806.
[35] G. C. Chinchen, K. C. Waugh, D. A. Whan, *Appl. Catal.* **1986**, *25*, 101–107.
[36] M. Rosenberg, P. Nicolaau, R. Manaila, P. Pausescu, *J. Phys. Chem. Solids* **1963**, *24*, 1419–1434.
[37] F. C. M. Driessens, G. D. Rieck, *Z. Anorg. Allg. Chem.* **1967**, *351*, 48–62.
[38] R. E. Vandenberghe, G. G. Robbrecht, V. A. M. Brabers, *Mater. Res. Bull.* **1973**, *8*, 571–580.
[39] A. D. D. Broemme, V. A. M. Brabers, *Solid State Ionics* **1985**, *16*, 171–178.
[40] M. Rydén, E. Cleverstam, M. Johansson, A. Lyngfelt, T. Mattisson, *AIChE J.* **2010**, *56*, 2211–2220.
[41] M. Arjmand, A.-M. Azad, H. Leion, A. Lyngfelt, T. Mattisson, *Energy Fuels* **2011**, *25*, 5493–5502.
[42] M. Arjmand, A.-M. Azad, H. Leion, A. Lyngfelt, T. Mattisson, *Ind. Eng. Chem. Res.* **2012**, *51*, 13924–13934.
[43] P. Cho, T. Mattisson, A. Lyngfelt, *Fuel* **2004**, *83*, 1215–1225.
[44] D. Kuuni, O. Levenspiel, *Fluidization Engineering*, 2nd Ed., Butterworth-Heinemann, Boston, **1991**.

Received: August 24, 2012
Revised: October 21, 2012

